Computer simulation of orthodontic tooth movement using CT image-based voxel finite element models with the level set method

Hasegawa, Masakazu; Adachi, Taiji; Takano-Yamamoto, Teruko

Computer Simulation of Orthodontic Tooth Movement Using CT Image-based Voxel Finite Element Models with the Level Set Method

Masakazu Hasegawa[1], Taiji Adachi[2,3], Teruko Takano-Yamamoto[4]

1: Division of Orthodontics and Dental Orthopedics, Graduate School of Dentistry, Tohoku University, Aoba, Sendai 980-8575, Japan
m-hasegawa@dent.tohoku.ac.jp

2: Department of Biomechanics, Institute for Frontier Medical Sciences, Kyoto University, Sakyo, Kyoto 606-8507, Japan
adachi@frontier.kyoto-u.ac.jp

3: Department of Micro Engineering, Graduate School of Engineering, Kyoto University, Sakyo, Kyoto 606-8501, Japan

4: Division of Orthodontics and Dental Orthopedics, Graduate School of Dentistry, Tohoku University, Aoba, Sendai 980-8575, Japan
t-yamamo@m.tohoku.ac.jp

Corresponding Author:

Professor Taiji Adachi PhD

Department of Biomechanics

Institute for Frontier Medical Sciences

Kyoto University

53 Kawahara-cho, Shogoin, Sakyo, Kyoto 606-8507, Japan
Tel & Fax: +81 (75) 751-4853
E-mail: adachi@frontier.kyoto-u.ac.jp

Submitted to Computer Methods in Biomechanics and Biomedical Engineering

Words: 4,794

Abstract:

Orthodontic tooth movement (OTM) is an adaptive biomechanical response of dentoalveolar components to orthodontic forces, in which remodeling of the alveolar bone occurs in response to changes in the surrounding mechanical environment. In this study, we developed a framework for OTM simulation by combining an image-based voxel finite element (FE) method, with a surface-tracking level set method using three-dimensional computer models. For a case study to demonstrate its capability of expressing clinical tooth movement, we observed displacement and rotation of the tooth under three types of force conditions. The simulation results demonstrate the proposed simulation method has the potential to predict clinical OTM.

Keywords: Tooth movement, Orthodontics, Level set method, Image-based model, Voxel finite element models, Computational biomechanics

1. Introduction

Orthodontic tooth movement (OTM) is a phenomenon that results from adaptive responses of the dentoalveolar components, namely teeth, alveolar bone, and the periodontal ligament (PDL), to applied orthodontic forces. In this process, remodeling of the alveolar bone occurs in response to changes in the surrounding mechanical environment (Wise & King 2008), in which a series of cellular activities, including osteoclastic bone resorption and osteoblastic osteoid deposition, is induced by cytokines released from the PDL (Rygh et al. 1986; Bister & Meikle 2013). To better understand the mechanism of OTM, evaluation of the complex mechanical environment of the dentoalveolar components under orthodontic forces is necessary.

For quantitative evaluation of the mechanical environment of the dentoalveolar components, a finite element (FE) method was introduced in the field of dental biomechanics research in the 1970s (Farah et al. 1973). Since then, FE analysis has rapidly spread because of its versatility in evaluating complex mechanical conditions, which cannot be directly measured in vivo (Limbert et al. 2010; Kida & Adachi 2014). Moreover, the development of medical imaging and visualization techniques involving X-ray computed tomography (CT) has provided powerful tools to integrate the vast amount of data from human bodies. These techniques enable us to reconstruct three-dimensional (3D) image-based computer models that can be directly applied to FE analysis; therefore, they are expected to contribute to further studies in various medical fields for more detailed and precise analyses.

In the field of orthodontics, appropriate treatment relies heavily on the personal experience of each clinician because of individual patient variability. Therefore, the development of a reliable tooth movement simulator is highly desirable. Studies have been conducted on OTM simulation by assessing various parameters that are driving factors behind tooth movement, such as stress and strain in alveolar bone (Bourauel et al. 2000; Provatidis 2006; Kojima et al. 2007). .

In this study, we propose a novel computer simulation framework for OTM using a combination of the 3D FE method and a level set method. The level set method (Osher & Sethian 1988) is a general interface tracking algorithm that enables us to handle changes in body shape and movement numerically, in which the surface boundary is represented by a level set function. Therefore, the FE level set method combination enables us to express tooth movement with detailed surface information. Using this novel framework, we conducted a case study to demonstrate its applicability. We employed the classic pressure-tension theory, one of the major hypotheses for OTM, on which current orthodontic studies are primarily based (Bister & Meikle 2013). Using the proposed method, we simulated a lower second premolar model under three types of forces representing clinical orthodontic situations.

2. Materials and Methods

2.1 Mathematical models of OTM based on the pressure-tension theory

As a case study, we applied the pressure-tension theory (Oppenheim 1911) as a hypothetical model of tooth movement under orthodontic forces. This theory is a bone remodeling hypothesis that can account for changes observed in alveolar bone during OTM. Current studies in orthodontics investigating the mechanism of bone and tissue metabolism during OTM mainly stand on the concept of this hypothesis, in which the compression of the PDL causes bone resorption and tensional deformation of the PDL causes bone deposition(Thiago et al. 2008).

We proposed a simple mathematical model of bone remodeling for tooth movement simulation based on the pressure-tension theory. According to in vitro observations, osteoclastic cells migrate to the site where the PDL is compressed (Rody et al. 2001). Therefore, we assume that the mechanical stimulus in the PDL is a driving factor for bone

remodeling on the pressure side. On the tension side, the PDL is disrupted by tensile force, leading to new bone apposition (Ahn et al. 2014). In this study, we assumed that bone and PDL are incrementally added to the tension side along with tooth movement. An osteoclastic cell induction factor was defined as the compressive strain normal to the PDL surface, $\varepsilon_n(\boldsymbol{X}_{PDL})$, at the position $\boldsymbol{X}_{PDL}$ in the PDL under orthodontic forces $\boldsymbol{F}$, as illustrated in Fig.1A and B.

During bone remodeling, osteoclastic cells resorb alveolar bone by acidification and proteolysis of the bone matrix (Hadjidakis & Androulakis 2006). Therefore, it can be assumed that the apparent bone density on the pressure side decreases because of bone resorption. In addition, we assumed that there is a certain distance within which osteoclastic cells can elicit a local response to PDL compression (Wolf et al. 2013). The rate of apparent bone density change $\rho_B(\boldsymbol{X}_B)$ by resorption is modeled as

$$\frac{\partial \rho_B(\boldsymbol{X}_B)}{\partial t} = \int_{PDL} \omega(l) f(\varepsilon_n(\boldsymbol{X}_{PDL})) dV, \quad (1)$$

depending on the strain $\varepsilon_n(\boldsymbol{X}_{PDL})$, where $\boldsymbol{X}_B$ is a position in the bone as shown in Fig.1C, $f(\varepsilon_n(\boldsymbol{X}_{PDL}))$ is a bone resorption function associated with strain $\varepsilon_n(<0)$ in the PDL, l denotes a distance from $\boldsymbol{X}_B$ to the point in the compressed PDL, $\boldsymbol{X}_{PDL}$, and $\omega(l)$ is a weight function:

$$\omega(l) = \begin{cases} (L-l)/L & (l \le L) \\ 0 & (L < l) \end{cases} \quad (2)$$

where L is the distance within which signals from the PDL are distributed to the resorption site.

The bone resorption function $f(\varepsilon_n(\boldsymbol{X}_{PDL}))$ is modeled as

$$f(\varepsilon_n(\boldsymbol{X}_{PDL})) =$$

$$\begin{cases} \alpha\varepsilon_{\mathrm{th2}} & (\varepsilon_{\mathrm{n}}(\boldsymbol{X}_{\mathrm{PDL}}) < \varepsilon_{\mathrm{th2}}) \\ \alpha\varepsilon_{\mathrm{n}}(\boldsymbol{X}_{\mathrm{PDL}}) & (\varepsilon_{\mathrm{th2}} \le \varepsilon_{\mathrm{n}}(\boldsymbol{X}_{\mathrm{PDL}}) < \varepsilon_{\mathrm{th1}}) \\ 0 & (\varepsilon_{\mathrm{th1}} \le \varepsilon_{\mathrm{n}}(\boldsymbol{X}_{\mathrm{PDL}}) < 0) \end{cases} \quad (3)$$

where $\varepsilon_{\mathrm{th1}}$ and $\varepsilon_{\mathrm{th2}}$($\varepsilon_{\mathrm{th2}}<\varepsilon_{\mathrm{th1}}<0$) are both thresholds of compressive strain, and α(>0) is a coefficients. Clinical studies demonstrate that there is an optimal force range for OTM, below which tooth movement does not occur and above which the rate of tooth movement becomes constant (Burstone 1988) . It also has been reported previously in the literature that the biological markers of bone remodeling as well as the rate of tooth movement are proportionate in some degree to the magnitude of the orthodontic force (Rohaya et al. 2013).

The bone mineral content affects the material properties of bone (Follet et al. 2004). Therefore, here we assume that the elastic properties of bone E_{B} as an isotropic material depend on its apparent bone density $\rho_{\mathrm{B}}(\boldsymbol{X}_{\mathrm{B}})$ using a conventional power's law with a constant γ(>0) based on previous literature (Morgan et al. 2003):

$$E_{\mathrm{B}}(\rho_{\mathrm{B}}) = E_{\max}(\rho_{\mathrm{B}}/\rho_{\max})^{\gamma} \qquad (0 < \rho_{\mathrm{B}}(\boldsymbol{X}_{\mathrm{B}}) \le \rho_{\max}), \quad (4)$$

where $E_{\max}$ denotes Young's modulus at the maximum bone density $\rho_{\max}$, which we obtained from the literature (Uddanwadiker et al. 2007). The value of γ was also obtained from a previous report (Morgan et al. 2003). By using equation 4, we represent the behavior of bone remodeling during OTM. As described in equations 1–4, the applied orthodontic force increases osteoclastic activity in the alveolar bone, which leads to bone resorption, in the range of osteoclast migration driven by compression of the PDL. Consequently, the tooth moves toward the bone-resorbed space with a small displacement $\boldsymbol{U}_{\mathrm{ortho}}$ (Fig.1D).

2.2 Tooth movement using the level set method with the voxel FE method

The use of the voxel FE method has the major advantage of building large-scale models with small computational costs (Adachi et al. 2006). In this study, the level set method (Osher & Sethian 1988) was employed to describe smooth tooth movement on a fixed voxel grid. The level set method is an interface tracking method used to handle the time-dependent movement of a curved surface by representing it with a function of one higher dimension than the original problem. The level set method has the advantage that the domain occupied by material at each moment of time is apparent from the sign of the level set function. The signed distance function, $\varphi(\boldsymbol{X},t)$, was defined as the level set function representing the tooth surface, and it has positive and negative values indicating external and internal regions of the tooth, respectively.

The movement of a tooth as rigid body motion is expressed by the level set equation:

$$\frac{\partial \varphi(\boldsymbol{X},t)}{\partial t} + F^{\varphi}(\boldsymbol{X})|\nabla \varphi(\boldsymbol{X},t)| = 0, \quad (5)$$

where F^{φ}(X) is a speed function representing the velocity of tooth movement under an orthodontic force $\boldsymbol{F}$ that is proportionally determined on the basis of tooth displacement $\boldsymbol{U}_{\mathrm{ortho}}$ obtained by FE analysis under the orthodontic force. The speed of evolution of the level set function was adjusted with F^{φ}(X), because the tooth shape represented by level set function tends to deform if evolution is too fast.

In this study, we updated the material properties of the FE models in the alveolar bone with altered bone elasticity as a result of bone remodeling by using equations 3 and 4, and $\varepsilon_{\mathrm{n}}(\boldsymbol{X}_{\mathrm{PDL}})$ of FE model. Using the voxel FE model with updated material properties at each iteration step, we estimated a small displacement of tooth $\boldsymbol{U}_{\mathrm{ortho}}$ caused by PDL deformation and bone remodeling. Level set function for tooth movement was evolved after determining the speed function of the level set by $\boldsymbol{U}_{\mathrm{ortho}}$, and at each iteration step, the tooth position of the FE model was updated in a step-wise manner on the basis of $\boldsymbol{U}_{\mathrm{ortho}}$ using a level set function.

2.3 Examination of model and boundary conditions

To examine the validity of the proposed simulation method, we conducted a case study using a simple model (Fig.2). A tooth was modeled as an assembly of an upper-half spherical body with a radius of 3.0 mm and a lower-half ellipsoid body with a semi-major axis of 4.5 mm (Fig.2A). By attaching 225-μm (3 voxels) thick PDL elements to half the height of the surface of the tooth model from the bottom and embedding the tooth model in a regular hexahedron bone model (70×66×48 voxels), a simple tooth‐alveolar bone complex model was constructed (Fig.2B).

This model was divided into 75-μm voxels. We assumed that all three components, namely the tooth, the PDL, and alveolar bone, behave as isotropic elastic materials with Poisson's ratios of 0.3, 0.4, and 0.3, respectively, and Young's moduli of 18.6 GPa, 0.17 MPa, and 13.7 GPa, respectively (Uddanwadiker et al. 2007). As a boundary condition, an orthodontic force of $F = 1.0$ N was applied to this model in the positive direction of the X-axis at a point located 1.5 mm from the top (Fig.2B). All nodal displacement was fixed on the bottom X‐Y plane, and normal displacement on the lateral walls (Y‐Z and Z‐X planes) of the alveolar bone model was fixed under shear-free conditions. The FE analysis was conducted using in-house software developed by the authors. In-house software was coded in Fortran and solver was element-by-element preconditioning conjugated gradient method.

2.4X-ray CT image-based model and applied force conditions

Three dimensional image-based models of the lower-right canine, second premolar, and first molar were constructed based on the procedures below. A 16-bit gray scale of each pixel in the CT DICOM data of the human lower mandible was extracted (Fig.3A). Each

image slice was binarized and segmented into hard tissues, such as tooth or alveolar bone, and other tissue using a manually determined threshold value. Tooth and alveolar bone were segmented at the PDL. Binarized images were reconstructed as a 3D image-based model (Moreira et al. 2012) (Fig.3B).

PDL elements 500 μm thick were attached to the root surface of each tooth model (Fig.3C), and placed into the alveolar bone element (Fig.3D). The elements of tooth, PDL, and alveolar bone were assumed to be in contact with each other as in the normal anatomical structure. Alveolar bone generally consists of cortical bone, trabecular bone, and alveolar bone proper. In this study, we assumed that the alveolar bone comprised homogeneous alveolar bone proper. The positive *X*-axis was set as the distal direction (Fig.3D), the positive *Y*-axis as the buccal direction, and the positive *Z*-axis as the crown direction.

The image-based model was 15.0 mm × 21.25 mm × 23.75 mm and divided into 352,119 voxel FEs of 250 μm with 1,126,941 degrees of freedom. We employed eight-node isoparametric element for FE analysis. As the initial value, all materials constituting bone, tooth, and PDL were assumed to be homogeneous, isotropic, linear elastic materials with Young's moduli of 13,700, 18,600, and 0.17 MPa, respectively, and Poisson's ratios of 0.3, 0.3, and 0.4, respectively (Uddanwadiker et al. 2007). The space inside the tooth was assumed to be filled with dental pulp and was treated as a cavity.

As a boundary condition, the bottom of the alveolar bone was fixed, and normal displacement at the lateral (distal and mesial) sides of the bone was assumed to be 0 (Fig.4). To simulate a clinical situation, we used three boundary conditions (Models M_{UT}, M_{TR}, and M_{CT}). In Model M_{UT} (Fig.4A), a 1.4 N external force ($\boldsymbol{F}_{UT}$) was applied to the buccal surface of the tooth crown in a mesial direction, causing an uncontrolled tipping movement of the tooth. In Model M_{TR} (Fig.4B), a force ($\boldsymbol{F}_{TR}$) equivalent to a moment of 2.5×10^{-3} Nm was applied to the buccal surface of the tooth crown to generate rotational movement. Finally, in

Model M_{CT} (Fig.4C), a combination of two forces ($\boldsymbol{F}_{CT} = \boldsymbol{F}_{UT} + \boldsymbol{F}_{TR}$) was applied for a controlled tipping movement. In uncontrolled tipping, the tooth tends to inclined because the tooth root is surrounded by alveolar bone. Application of F_{CT} has a purpose of the retention of the inclination of tooth during tooth movement. These models simulated OTM and we observed the movement under each loading condition.

3. Result: Examination of mathematical model behaviors

3.1 Change in Young's modulus in alveolar bone caused by resorption

The distribution of the compressive strain $\varepsilon_n(\boldsymbol{X}_{PDL})$ in a normal direction in the PDL and the change in Young's modulus of the alveolar bone as evaluated by equations 1 and 4 along the simulation iteration are shown in Fig.5, in which one quarter of the PDL and bone elements were removed for observation (Fig.5A).

As a result of the simulation, the compressive strain was distributed in the cervical portion of the PDL in the direction of the force (Fig.5B). As the iteration steps progressed, the magnitude of compressive strain slightly increased without any significant change in the distribution pattern. Young's modulus of the alveolar bone in the vicinity of the PDL gradually decreased (Fig.5C) corresponding to compressive strain distribution (Fig.5B), which led to tooth movement.

The distribution pattern of normal strain in the normal direction (Fig.5B) was well correlated to with the change in bone density around the PDL (Fig.5C), indicating that bone resorption was successfully expressed in the proposed model. The pattern of change in bone elasticity in this model was typically observed in a histological study of tooth movement

(Collin et al. 2014). Therefore, our simulation method is capable of expressing tooth movement based on the mathematically expressed pressure-tension theory.

3.2 OTM simulation using an image-based model

As a result of the tooth movement simulation, the tooth moved with displacement and rotation (inclination) according to each applied force (Fig.6). The amount of displacement on the *X*-*Z* plane was evaluated at the center of gravity of each tooth model. In Model M_{UT}, the tooth was displaced in a mesial direction, and its long axis was also inclined towards the mesial (Fig.6A). In the field of orthodontics, this type of movement is described as uncontrolled tipping. In the case of Model M_{TR}, the tooth inclined in a distal direction opposite to the movement observed in Model M_{UT}, and exhibited a small distal displacement (Fig.6B), described as torque movement in the field of orthodontics. In Model M_{CT}, the tooth exhibited mesial movement with inclination of the long axis in a mesial direction (Fig.6C), although the magnitude of the inclination change was smaller than in Model M_{UT}. Therefore, the simulation results showed that the inclination change decreased and the translocation was controlled in Model M_{CT}, in a process described as controlled tipping.

Change in the inclination of the tooth axis in the X–Z plane θ_t and the displacement of the center of gravity d_t observed in each model are plotted in Fig.7. In Models M_{UT} and M_{CT}, the tooth moved in a mesial direction and the tooth axis inclined in the X–Z plane. The inclination of the tooth axis in Model M_{CT} decreased to approximately half that in Model M_{UT}. These simulations demonstrate that we can predict OTM that depends on applied forces, suggesting that it would be possible to apply this simulation framework to quantitative predictions for more practical use.

4. Discussion

In this study, we developed a novel orthodontic simulation framework using image-based voxel FE models combined with the level set method. To improve the predictability of treatment, OTM simulations have been conducted under various mechanical conditions with various bone-remodeling constitutive models (Bourauel et al. 2000; Kojima et al. 2007). These simulation results corresponded to clinical tooth movement. However, in these simulations, a process to integrate the step-wise displacement of the tooth, consisting of a huge number of FE nodes, into total tooth movement required time-consuming procedures such as iterative re-meshing of the FE models on the basis of nodal displacement of each FE at each simulation step, keeping the tooth shape undeformed. Thus, a novel method for tooth movement simulation that is applicable to clinical situations is required. In present study, we employed the level set method, which is a surface tracking technique, to move a tooth as a rigid body within the PDL/alveolar bone on the basis of nodal displacement owing to its elastic deformation under a virtual orthodontic force. In our method, the level set function is updated to express the displacement of the curved tooth surface. In this manner, we were able to simulate tooth movement smoothly.

In addition to employment of the level set method, we applied 3D CT image-based models for FE analysis, using a 16-bit gray scale to determine threshold of the binarization. The previous study reported a strong correlation between gray scale and Hounsfield units (Tahmineh et al. 2014). Therefore, we consider that gray scale is sufficient for construction of an image-based model. The CT image-based model enables us to conduct FE analysis with a more precisely replicated individual jaw model. Furthermore, image-based voxel FE method has the significant advantage that the CT or MR images can be directly converted into eight-node hexahedral FE, and an explicit mathematical representation of the geometry is not required (Keaveny et al. 2001). Therefore, the image-based voxel FE reduces the time-

consuming procedures required to produce simulation (Francisco et al. 2014). For the clinical application of the numerical simulation studies including our framework, the further reduction of computational cost becomes a task to accomplish. We believe that the strength of voxel FE described above will aid in the clinical application of our simulation framework.

Guldberg et al. (1998) suggested that the use of voxel element with one-fourth the size of the analyzed object showed good numerical convergence behavior on trabecular bone. Crawford et al. (2003) and Majid et al. (2014) demonstrated that the voxel FE model predicted the stiffness in an excellent manner regardless of whether the voxel size was relatively large or small, with vertebrate model and femur model, respectively. In the preset study, we used much smaller voxel element compared to the simulation model, therefore, we believed that the numerical accuracy was ensured. Furthermore, the integrated form of analytical values obtained by equation 1 is expected to reduce the effect of the jagged voxel edge onto the whole simulation result to a minimum in our simulation framework.

In the present study, we conducted a case study with a proposed novel simulation framework to evaluate its applicability using an image-based FE model of human lower right teeth with alveolar bone. We focused to behavior of loaded tooth and adjacent alveolar bone because it becomes possible to apply orthodontic force without generating reaction force in adjacent teeth owing to the improvement of orthodontics. As the result of simulation, we successfully demonstrated its capability to qualitatively simulate orthodontics tooth movement patterns typically observed in clinical situations. In this framework, tooth movement was simulated based on step-wise linear movements in an iterative procedure. CT imaging techniques have been rapidly developing as an irreplaceable method of obtaining human internal information in a non-invasive manner. Therefore, it is expected that we will be able to conduct simulations with more detailed patient-specific models in the near future. However, it is expected that the parameters, such as alveolar bone volume and the nonlinear

properties of the PDL, which were simplified and/or excluded in the present study, will affect the simulation results. In addition, it is necessary to consider soft tissues (e.g., masticatory muscles) and the geometry of the mandiblular bone in construction of boundary conditions because they also affect tooth movement and bone remodeling (Ziegler et al. 2005; Van Schepdael et al. 2012). These parameters needs to be incorporated into the simulation and the model needs to be quantitatively validated through animal and clinical studies so that specific simulation models that are morphologically and biologically accurate can be developed for individual patients.

Evaluation of biological simulation models such as ours involves the important process of verification and validation. To apply these steps to the tooth movement simulation in the present study, a thorough clarification of the OTM mechanism is indispensable. However, the biological mechanism of OTM in alveolar bone is yet to be completely understood. In this study, we performed a simulation under the following simple assumptions. We assumed that the PDL strain was a driving force in bone remodeling under orthodontic forces and that apparent bone density decreases because of bone resorption. Various hypotheses exist for bone remodeling in tooth movement including pressure-tension, bone-bending (Grimm 1972), and bioelectric theories (Krishnan & Davidovitch 2009). Here, we employed the pressure-tension theory, which hypothesize that bone remodeling is mechanically activated by compression and tension in the PDL (Oppenheim 1911) because this concept has long dominated current orthodontic theories (Bister & Meikle 2013). However, the relationship between the driving mechanical factors and bone remodelling activity has not been quantitatively formulated. Therefore, in the present study, we simply assumed that activation of remodeling is linearly correlated with the magnitude of the compressive strain in the PDL within the range of some threshold values. The fundamental

constitutive law to express the rate of bone remodeling in OTM needs to be experimentally investigated. Recently, the mechanism of OTM

Further development of OTM simulation would provide quantitative estimates with increased accuracy for use in clinical applications such as prediction of tooth movement. In orthodontics, consideration of the center of resistance (CR) is indispensable for achieving precise OTM. Many researchers have estimated the loc has been studied in various ways (Benedetta et al. 2013; Fabrizia et al. 2013). The verification and validation of our simulation framework based on these findings will contribute to the understanding the mechanism of tooth movement in the future. ation of the CR with FE models in various clinical situations (Sung et al. 2010). However, its position shifts with remodeling of the surrounding alveolar bone. By using the developed simulation method, time-dependent change of the CR can be tracked. It could also be applied to optimize planning of the orthodontic force pattern and magnitude. Because our CT image-based model reflects details of the patient's specific tissue morphology, the simulation will contribute to establishing individual treatment planning. Therefore, development of OTM simulation for clinical application will assist clinicians in designing treatment plans and predicting treatment outcomes for individual patients.

Acknowledgment

This work was partially supported by Grants-in-Aid for Scientific Research from the Japan Society for the Promotion of Science (JSPS).

(Guldberg et al. 1998) (Crawford et al. 2003) (Majid et al. 2014)

References

Adachi T, Osako Y, Tanaka M, Hojo M, Hollister SJ. 2006. Framework for optimal design of porous scaffold microstructure by computational simulation of bone regeneration. Biomaterials 27(21):3964-72.

Ahn H, Ohe J, Lee S, Park Y, Kim S. 2014. Timing of force application affects the rate of tooth movement into surgical alveolar defects with grafts in beagles. American Journal of Orthodontics & Dentofacial Orthopedics 145(4):486-495.

Benedetta G, Marie-Christine dV, Caroline M-M, Fabio DL, Marco F, Luca M, Antonella F, Pascal H, Antonio R, Valerie G. 2013. Alteration of proteoglycan sulfation affects bone growth and remodeling. BONE 54:83-91.

Bister D, Meikle MC. 2013. Re-examination of 'Einige Beitrage zur Theorie der Zahnregulierung' (Some contributions to the theory of the regulation of teeth) published in 1904-1905 by Carl Sandstedt. Eur J Orthod 35(2):160-8.

Bourauel C, Vollmer D, Jager A. 2000. Application of Bone Remodeling Theories in the Simulation of Orthodontic Tooth Movements. Journal of Orofacial Orthopedics 61:266-279.

Burstone CJ. 1988. The biophysics of bone remodeling during orthodontics-optimal force considerations. The Biology of Tooth Movement, CRC Press.

Collin DK, Phillip MC, Robert S, Reginald WT, Peter HB. 2014. Bony adaptation after expansion with light-to-moderate continuous forces. American Journal of Orthodontics and Orthopedics 145(5):655-666.

Crawford R, Rosenburg W, Keaveny T. 2003. Quantitative Computed Tomography-Based Finite Element Models of the Human Lumbar Vertebral Body: Effect of Element Size on Stiffness, Damage, and Fracture Strength Predictions. Journal of Biomechanical Engineering 125:434-438.

Fabrizia dA, Salvatore C, Domenico C, Angela M, Armando S-B, Letizia P. 2013. Biomarkers of Periodontal Tissue Remodeling during Orthodontic Tooth Movement in Mice and Men: Overview and Clinical Relevance. The ScientificWorld Journal 2013:1-8.

Farah JW, Craig RG, Sikarski.Dl. 1973. Photoelastic and Finite-Element Stress Analysis of a Restored Axisymmetric First Molar. Journal of Biomechanics 6(5):511-520.

Follet H, Boivin G, Rumelhart C, Meunier PJ. 2004. The degree of mineralization is a determinant of bone strength: a study on human calcanei. Bone 34(5):783-789.

Francisco M-C, Jorge M-M, Fernando M. 2014. Mesomechanical characterization of porosity in cementitious composites by means of a voxel-based finite element model. Computational Materials Science 90:157-170.

Grimm FM. 1972. Bone bending, a feature of orthodontic tooth movement. Am J Orthod 62(4):384-93.

Guldberg R, Hollister S, Charras G. 1998. The accuracy of digital imagebased finite element models. J Biomech Eng 120:289-295.

Hadjidakis DJ, Androulakis II. 2006. Bone remodeling. Annals of the New York Academy of Sciences 1092:385-396.

Keaveny TM, Morgan EF, Niebur GL, Yeh OC. 2001. Biomechanics of Trabecular Bone. Annual Review of Biomedical Engineering 2001:307-333.

Kida N, Adachi T. 2014. Numerical analysis of arterial contraction regulated by smooth muscle stretch and intracellular calcium ion concentration. Journal of Biomechanical Science and Engineering 9(1):JBSE0002-JBSE0002.

Kojima Y, Mizuno T, Umemura S, Fukui H. 2007. A numerical simulation of orthodontic tooth movement produced by a canine retraction spring. Dental Materials Journal 26(4):561-567.

Krishnan V, Davidovitch Z. 2009. On a Path to Unfolding the Biological Mechanisms of Orthodontic Tooth Movement. Journal of Dental Research 88(7):597-608.

Limbert G, van Lierde C, Muraru OL, Walboomers XF, Frank M, Hansson S, Middleton J, Jaecques S. 2010. Trabecular bone strains around a dental implant and associated micromotions-A micro-CT-based three-dimensional finite element study. Journal of Biomechanics 43(7):1251-1261.

Majid M, Maziyar K, Vahid N. 2014. Analysis of strength and failure pattern of human proximal femur using quantitative computed tomography (QCT)-based finite element method. Bone 64:108-114.

Moreira AC, Appoloni CR, Mantovani IF, Fernandes JS, Marques LC, Nagata R, Fernandes CP. 2012. Effects of manual threshold setting on image analysis results of a sandstone sample structural characterization by X-ray microtomography. Applied Radiation & Isotopes 70(6):937-941.

Morgan EF, Bayraktar HH, Keaveny TM. 2003. Trabecular bone modulus-density relationships depend on anatomic site. Journal of Biomechanics 36(7):897-904.

Oppenheim A. 1911. Tissue changes, particularly of the bone, incident to tooth movement. American Orthodontist 3(56-67):113-132.

Osher S, Sethian JA. 1988. Fronts Propagating with Curvature-Dependent Speed - Algorithms Based on Hamilton-Jacobi Formulations. Journal of Computational Physics 79(1):12-49.

Provatidis CG. 2006. A Bone-Remodelling Scheme Based on Principal Strains Applied to a Tooth During Translation. Computer Methods in Biomechanics and Biomedical Engineering 6(5-6):347-352.

Rody WJ, King GJ, Gu GM. 2001. Osteoclast recruitment to sites of compression in orthodontic tooth movement. American Journal of Orthodontics & Dentofacial Orthopedics 120(5):477-489.

Rohaya M, Abdul, Wahab,, Maryati M, Dasor,, Sahidan S, Asma A, Abang, Abdullah, , Zulham Y, Abdul A, Jemain, , Shahrul H, Zainal, Ariffin. 2013. Crevicular Alkaline Phosphatase Activity and Rate of Tooth Movement of Female Orthodontic Subjects under Different Continuous Force Applications. International Journal of Dentistry 2013(2013).

Rygh P, Bowling K, Hovlandsdal L, Williams S. 1986. Activation of the Vascular System - a Main Mediator of Periodontal Fiber Remodeling in Orthodontic Tooth Movement. American Journal of Orthodontics & Dentofacial Orthopedics 89(6):453-468.

Sung SJ, Jang GW, Chun YS, Moon YS. 2010. Effective en-masse retraction design with orthodontic mini-implant anchorage: a finite element analysis. American Journal of Orthodontics & Dentofacial Orthopedics 137(5):648-57.

Tahmineh R, Mahdi N, Fakhri A, Ghazani. 2014. Relationship between Hounsfield Unit in CT Scan and Gray Scale in CBCT. Journal of Dental Research, Dental Clinics, Dental Prospects 8(2):107-110.

Thiago P, Garlet,, Ulisses C, Carlos E, Repeke,, João S, Silva, , Fernando d, Queiroz, Cunha, , Gustavo P, Garlet,. 2008. Differential expression of osteoblast and osteoclast chemmoatractants in compression and tension sides during orthodontic movement. Cytokine 42:330-335.

Uddanwadiker RV, Padole PM, Arya H. 2007. Effect of variation of root post in different layers of tooth: Linear vs nonlinear finite element stress analysis. Journal of Bioscience and Bioengineering 104(5):363-370.

Wise GE, King GJ. 2008. Mechanisms of tooth eruption and orthodontic tooth movement. Journal of Dental Research 87(5):414-434.

Wolf M, Lossdorfer S, Craveiro R, Gotz W, Jager A. 2013. Regulation of macrophage migration and activity by high-mobility group box 1 protein released from periodontal ligament cells during orthodontically induced periodontal repair: an in vitro and in vivo experimental study. J Orofac Orthop 74(5):420-434.

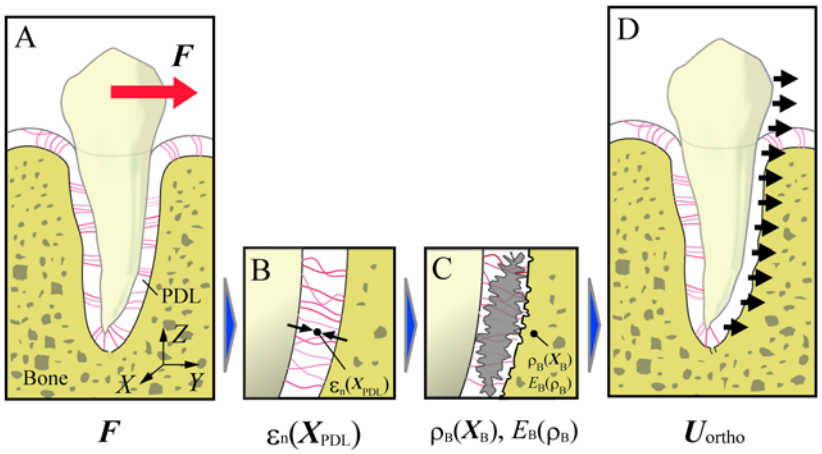

1 Figure 1: A model of orthodontic tooth movement.

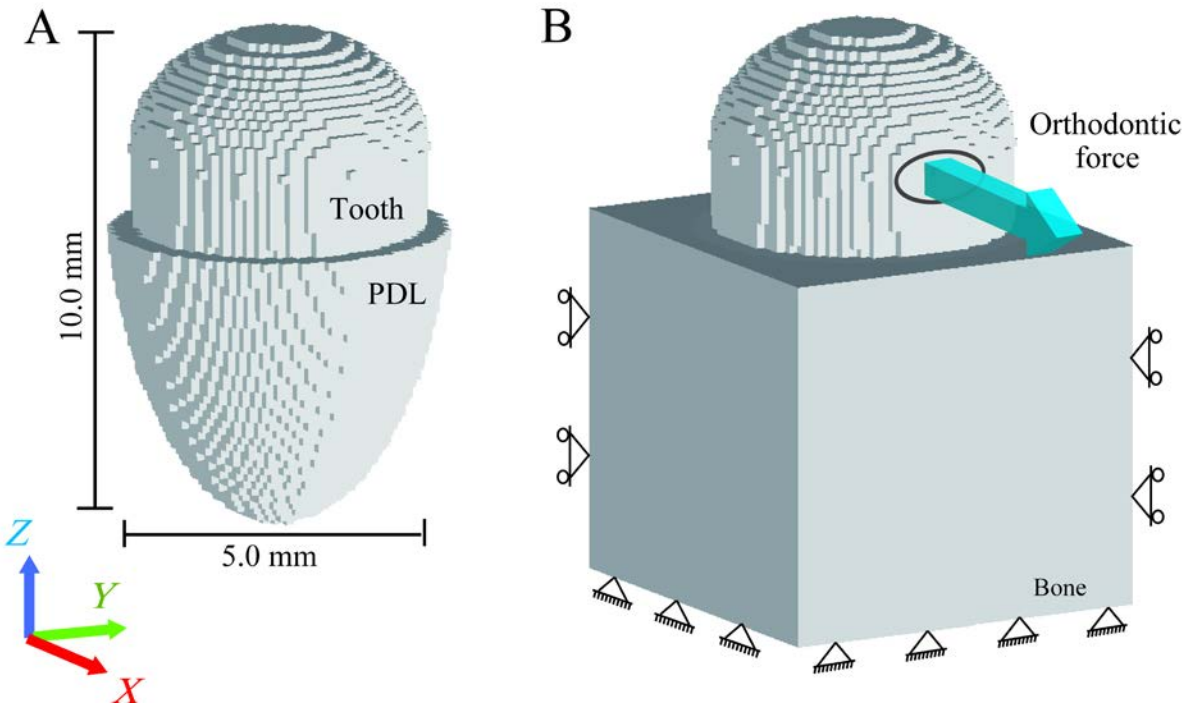

Figure 2: A simple model for investigating changes in bone density using the proposed simulation framework.

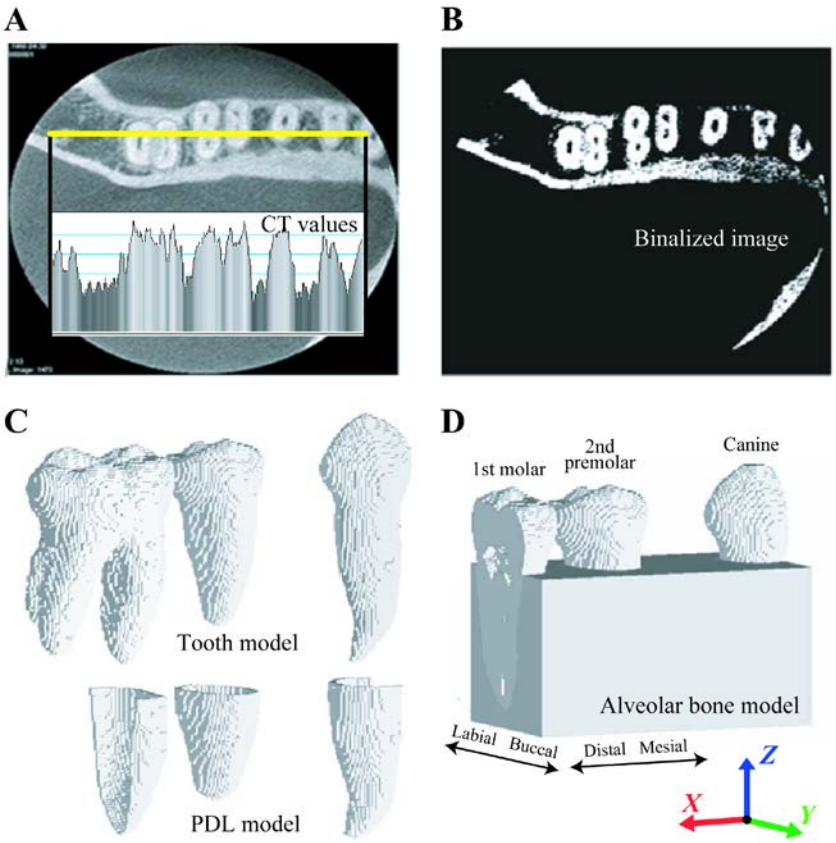

1 Figure 3: Construction of a CT image-based FE model.

2

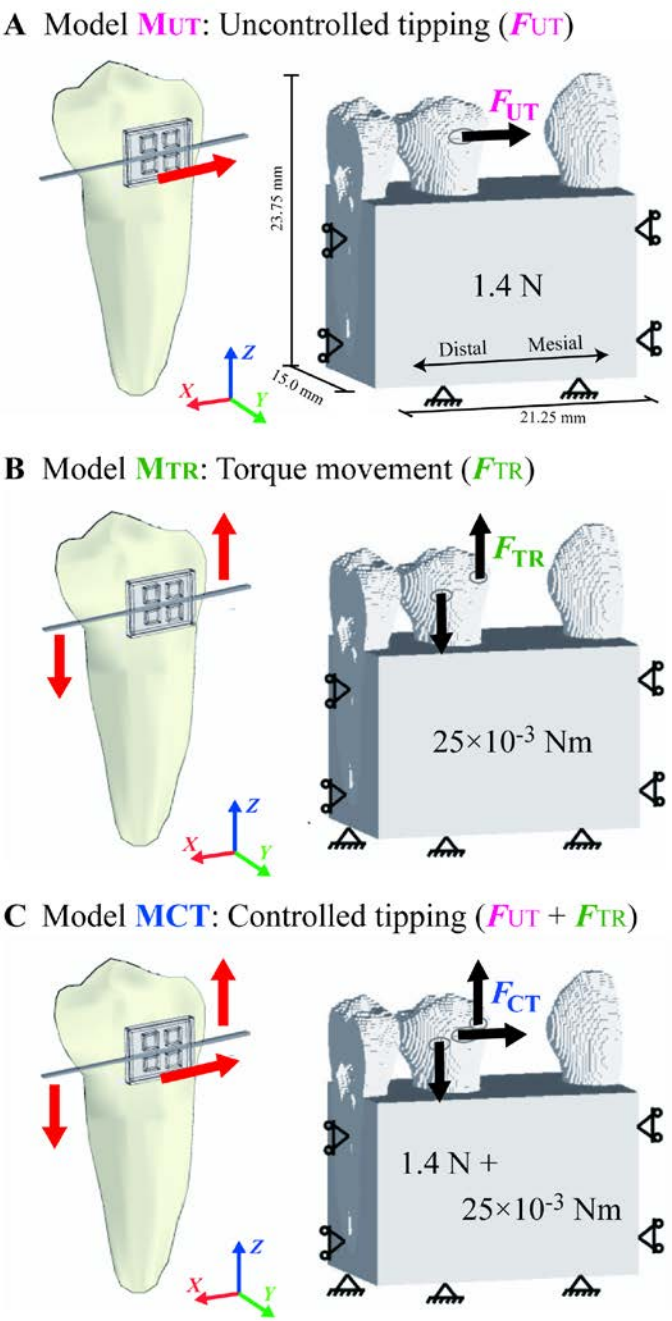

Figure 4: Boundary conditions for simulation of orthodontic tooth movement.

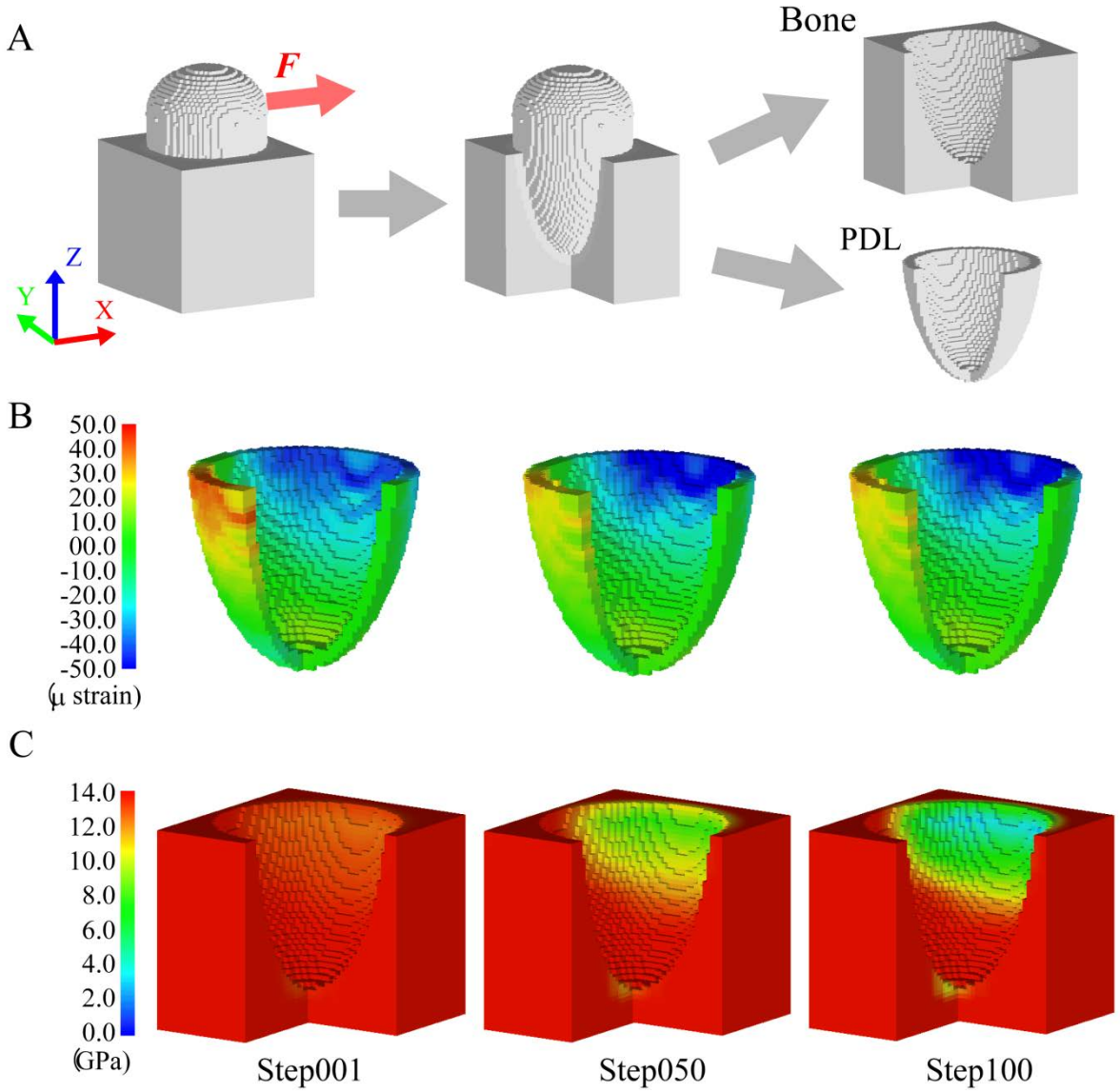

Figure 5: Orthodontic tooth model simulation for a simple tooth-alveolar bone model.

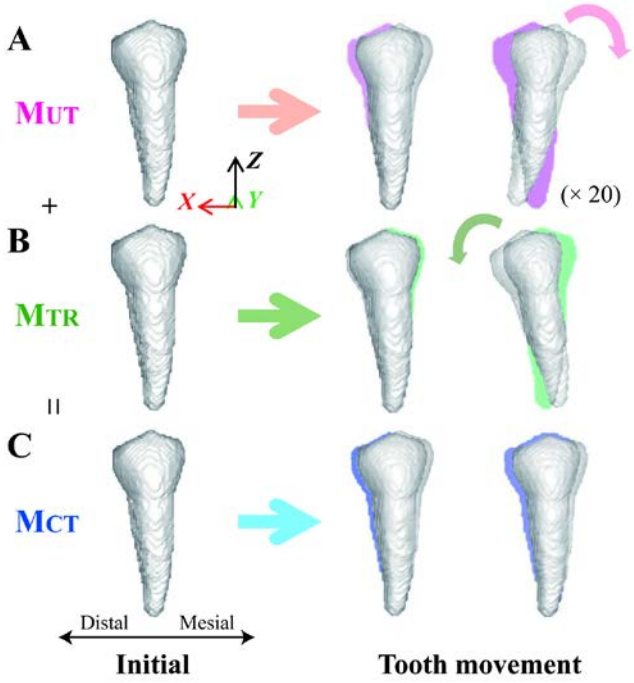

Figure 6: Tooth movement patterns simulated under different orthodontic force conditions.

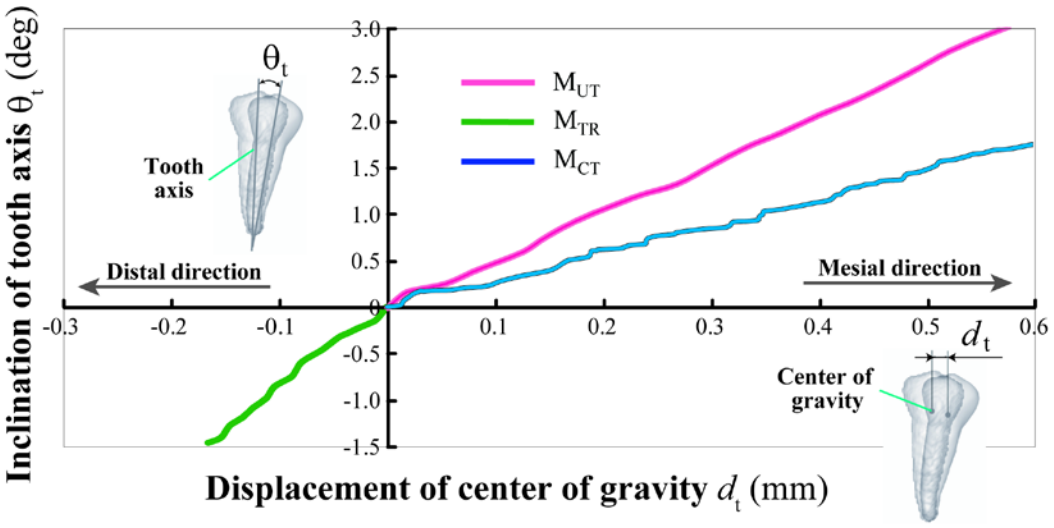

1 Figure 7: Tooth movement with displacement and inclination predicted by orthodontic tooth
2 movement simulation.

Figure Captions

Figure 1: A model of OTM.

(A) Application of an orthodontic force F, (B) compressive strain $\varepsilon_n(X_{PDL})$ in the normal direction n to the tooth surface at X_{PDL} in the PDL region, and (C) degradation of the PDL and remodeling of alveolar bone lead to a decrease in apparent bone density $\rho_B(X_B)$ because of bone resorption and results in a decrease in Young's modulus of the alveolar bone $E_B(\rho_B)$ at X_B, so that (D) the tooth moves with a displacement U_{ortho} under the orthodontic force F.

Figure 2: A simple model for investigating changes in bone density using the proposed simulation framework.

(A) A tooth model with PDL and (B) a tooth-alveolar bone complex model. The orthodontic force (F = 1.0 N) was applied in the positive direction of X axis. The gray circle indicate the location of orthodontic force $\boldsymbol{F}$.

Figure 3: Construction of a CT image-based FE model.

(A) A CT image of the human right mandibular bone was obtained using dental X-ray CT. Spatial resolution was 125 μm × 125 μm and slice thickness 125μm. The value contained in each pixel of the CT image was extracted. (B) Each slice image was binarized on the basis of the values extracted from the pixels, and the regions with values greater than the threshold value were assumed to be hard tissues such as bone and teeth. (C) Image-based models of the lower-right canine, second premolar, and first molar were constructed on the basis of a series of binarized images. Voxel size was isotropic 250 μm. PDL elements with a thickness of 500 μm were attached to the root surface of each tooth. (D) A simulation model was constructed by embedding model teeth into the homogenous alveolar bone element.

Figure 4: Boundary conditions for simulation of OTM.

(A) Uncontrolled tipping under a single tensile force F_{UT}. (B) Torque movement under a moment caused by F_{TR}. (C) Controlled tipping under forces $F_{CT} = F_{UT} + F_{TR}$. The gray circles indicate the location of each force.

Figure 5: Orthodontic tooth model simulation for a simple tooth-alveolar bone model.

(A) The model comprises tooth, PDL, and alveolar bone (quarter parts removed). (B) Distribution of normal compressive strain $\varepsilon_n(X_{PDL})$ in the PDL, and (C) changes in Young's modulus due to changes in apparent density caused by resorption of the alveolar bone.

Figure 6: Tooth movement patterns simulated under different orthodontic force conditions, superimposed with the initial positions and magnified 20 times.

(A) Model M_{UT} showed mesial movement along the force direction with significant inclination, a movement described as uncontrolled tipping. (B) Model M_{TR} showed tooth rotation in the opposite distal direction and a small distal movement, a movement described as torque movement. (C) Model M_{CT} showed mesial movement with a smaller inclination compared with Model M_{UT}, a movement described as controlled tipping.

Figure 7: Tooth movement with displacement and inclination predicted by OTM simulation for Models M_{UT} (magenta), M_{TR} (green), and M_{CT} (blue). Displacement d_t in the X-axis direction was evaluated at the center of gravity of the tooth model, and inclination θ_t was measured as the rotation of the long axis projected onto the Z-X plane.